Int J Adv Manuf Technol (2010) 48:461–472
DOI 10.1007/s00170-009-2318-y

ORIGINAL ARTICLE

A manufacturing model of an end mill using a five-axis CNC grinding machine

Trung Thanh Pham · Sung Lim Ko

Received: 9 April 2009 / Accepted: 15 September 2009 / Published online: 8 January 2010

Abstract This paper presents a manufacturing model of a flat-end mill using a five-axis computer numerical control (CNC) grinding machine. The profile of the helical groove can be precisely calculated using a given wheel profile and the relative movements between the workpiece and the grinding wheel. The results of the calculation of the numerical control (NC) data for all the grinding processes of the end mill are fully presented in the paper. The NC data for the machining end mill were generated from the developed program by using the given design parameters of tool geometry, wheel geometry, wheel setting, and machine setting. The effects of the design and manufacturing of the end mill were analyzed based on the computer simulation and experiment results. This study provides a practical and efficient model for the manufacturing of an end mill using a CNC grinding machine with simple programming techniques. The prediction of the end mill geometry for the designing of the proper configuration of the end mill before manufacturing and generating the NC code for machining in a CNC machine is necessary to save time and to reduce the manufacturing cost.

T. T. Pham
Department of Advanced Technology Fusion, Konkuk University,
1 Hwayang-dong, Kwangjin-gu,
Seoul 143-701, South Korea

S. L. Ko (✉)
Department of Mechanical Design and Production Engineering,
Konkuk University,
1 Hwayang-dong, Kwangjin-gu,
Seoul 143-701, South Korea
e-mail: slko@konkuk.ac.kr

Keywords End mill · Helical groove · Cutting tools · CNC grinding

1 Introduction

End mills are widely used in industry for high-speed machining. The grinding of an end mill with a complex geometry is related to some complicated processes in machining with a CNC grinding machine. Therefore, the research on helical-groove grinding and cutting tool manufacturing has drawn the interest of many researchers. Kang et al. [1] proposed a mathematical model for helical-groove machining that is based on the establishment of the fundamental analytical conditions of engagement between the generating tool surface and the helical-groove surface. Several mathematical approaches have been developed for helical-groove machining and complex-shaped cutters manufacturing such as ball-end mill, taper ball-end mill, and concave cone-end milling cutters [2–9]. The mathematical models, however, which are related to a number of complicated programming techniques, deal with complicated mathematics and analytical differential geometry and kinematics using a computer and require that the desired surface profiles be continuous. Most of the related works that have been carried out on the aforementioned topics are concerned with the design and machining of the helical-groove and cutting-edge curves. There are many kinds of end mills with complex shapes, and it is not easy to accurately obtain the mathematical models of tool geometry for the simulation of the grinding process.

In these authors' previous work [10], a model for the geometric analysis of helical-flute grinding was proposed, and a software for determining the grinding wheel

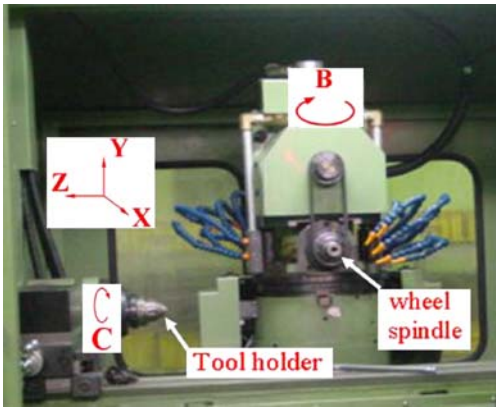

Fig. 1 The five-axis CNC grinding machine for end mill manufacturing

geometry and the setting condition was developed. This study presents a practical and efficient model for manufacturing an end mill using a five-axis CNC grinding machine with simple programming techniques. The NC data for the grinding end mill will be generated from the developed software and will be used for designing and predicting the proper end mill geometry before machining.

2 Development of a software for manufacturing a grinding end mill

In this study, an end mill was machined using a five-axis CNC grinding machine. Figure 1 shows the configuration of the five-axis CNC grinding machine with 5 degrees of freedom: three axes in translation (X, Y, Z) and two in rotation (B, C). Four kinds of grinding wheels were used for machining the end mill. There are four main machining operations for end mill manufacturing: fluting, first and second clearance faces, gash face, and the first and second end teeth face grinding processes. Figure 2 shows a schematic diagram of the machine setting, the arrangement of the grinding wheels on the wheel spindle, and the wheel geometry for end mill manufacturing. The machine setting parameters, end mill geometric parameters, wheel settings, and wheel geometry must be measured and inputted into the program in advance.

2.1 End mill geometry

In general, the geometry of a flat-end mill consists of two parts: the geometry of the flute surface and that of the end surface. The flute surface can be obtained by combining rotational and parallel sweeping. Shown in Fig. 3 are some of the many design factors in end mill manufacturing: diameter (D), inscribed-circle diameter (D_i), rake angle (γ), clearance angles (η), helix angle (h_e), gash angle (θ_g), and end teeth angles (ε).

In this research, the rake and clearance angles were defined as the tangential angle at the edge. The rake and clearance angles are the most important among the design factors. The rake angle, in particular, affects the stiffness of the cutting edge and the rigidity of the tool. An end mill with a positive rake angle has better machining ability, thereby producing a lower cutting force and cutting temperature. In general, it is the positive rake angle that is applied to the conventional

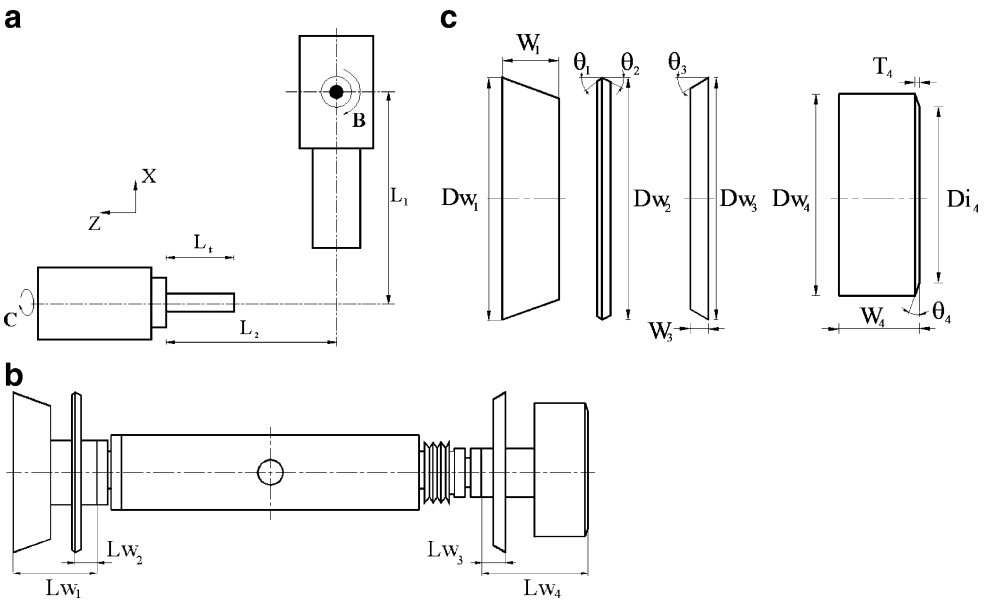

Fig. 2 **a** Schematic diagram of the machine setting, **b** arrangement of the grinding wheels on the wheel spindle, **c** wheel geometry

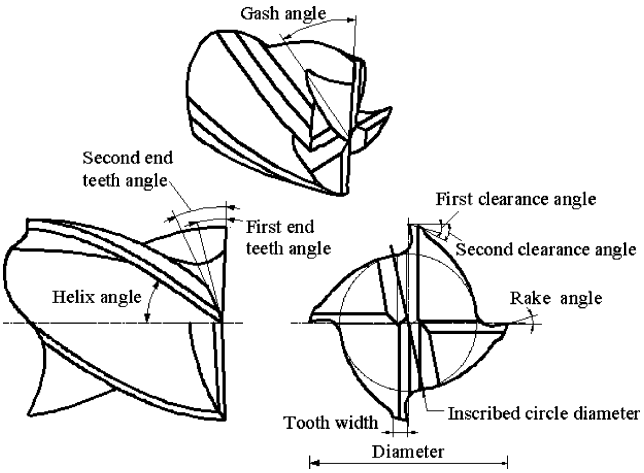

Fig. 3 The design parameters of the end mill

end mill. In the case of the negative rake angle, the stiffness of the cutting edge is increased, and the chipping is suppressed [11].

The cutting angle of an end mill is very important in the latter's design and analysis. In this study, general formulas for all the cutting angles of end mills were derived depending on the relationship between the grinding wheel movement and the geometric design parameters.

2.2 Helical-flute grinding and calculation of the grinding data

The combined motion of the grinding wheel and the workpiece generates the helical-groove surface. The flute surface of the end mill can be represented by the helical motion of the cross section, and the configuration of the flute shape is related to the shape of the grinding wheel. The simulation algorithm for the helical-groove machining in this study was based on the assumption that a wheel with a finite thickness consists of a finite number of thin disks. The profile of the helical groove can be calculated uniquely and exactly if an exact wheel profile will be used as an input. By accumulating the points met by each thin disk with each sleeve of the workpiece, the helical groove was predicted using the wheel profile [10].

Figure 4 shows the schematic illustration of the fluting operation. The computer program will determine the contact point between the circle and the ellipse, which is

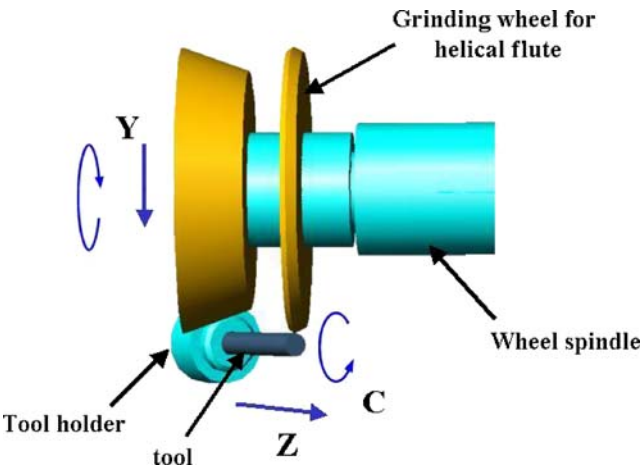

Fig. 4 Schematic illustration of the fluting operation

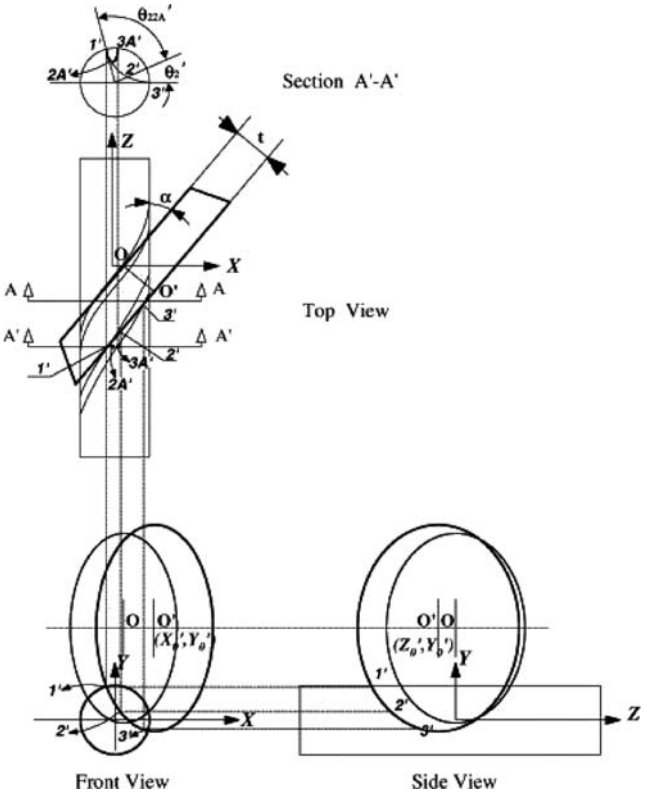

Fig. 5 The algorithm for finding the cross-sectional profile of the helical flute

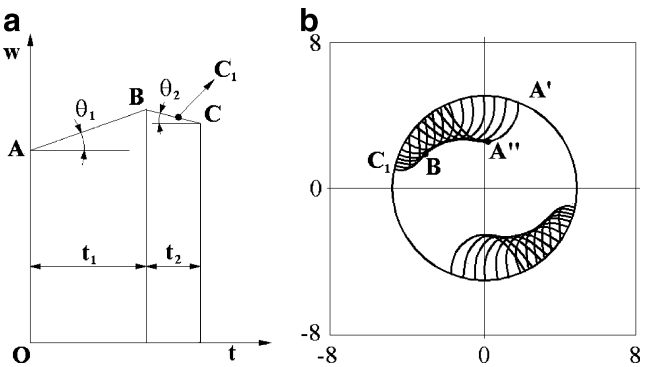

Fig. 6 **a** Configuration of the grinding wheel and **b** flute shapes of the end mill

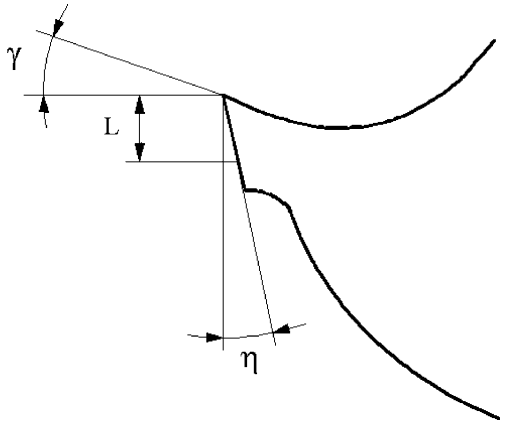

Fig. 7 The cross-sectional plane of the flute, rake, and clearance angles

the projection of the wheel on the normal plane towards the axial direction of the end mill. In this case, the diameter of the end mill and the *Z*-axis of the wheel location are fixed, and only the *Y*-axis of the wheel is changed to find the contact point. The flute configuration was generated from the cross-points between the given grinding wheel and the end mill. The cross-point between the wheel and the outer diameter of the end mill was used as a reference point to configure the flute shape and to calculate the grinding points for the clearance faces, end teeth faces, and gash face.

Figure 5 shows the algorithm for finding the cross-sectional profile of the helical flute. To find the groove configuration in cross section A–A, the grinding wheel and

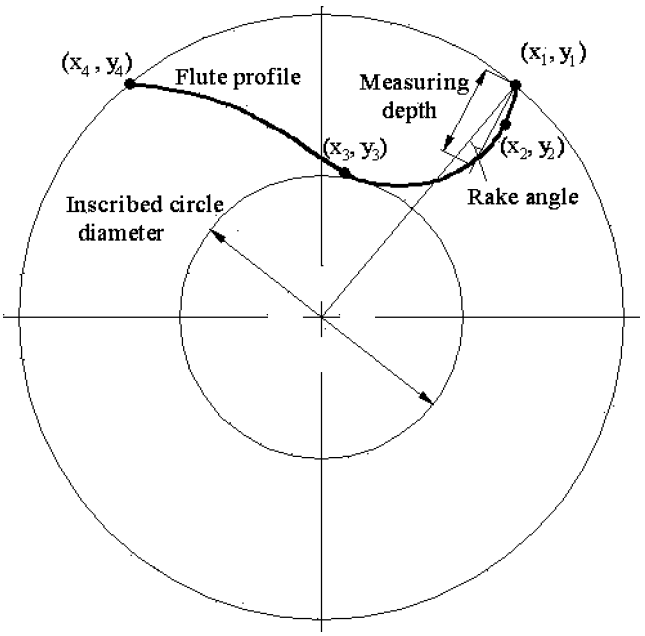

Fig. 8 The configuration of the cross-sectional flute

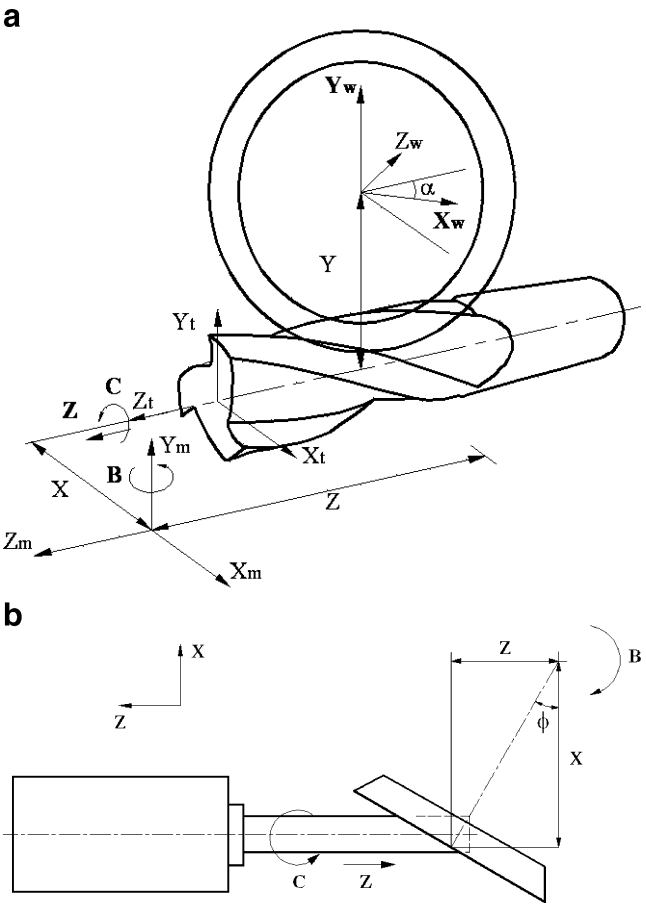

Fig. 9 **a**, **b** Schematic diagram of the helical-flute grinding process

the workpiece can be represented in the *X*–*Y* and *Y*–*Z* coordinates by using the following equations:

$$\frac{(x-x_0)^2}{(w\sin\alpha)^2}+\frac{(y-y_0)^2}{w^2}=1 \tag{1}$$

and

$$\frac{z^2}{(w\cos\alpha)^2}+\frac{(y-y_0)^2}{w^2}=1. \tag{2}$$

The workpiece can be represented by the following equation:

$$x^2+y^2=R^2, \tag{3}$$

where (x_0, y_0) is the given wheel center position.

The three points 1, 2, and 3 are located on the grinding wheel. Two points (x_0, y_0) in the front views (x_1, y_1) and (x_3, y_3) can be obtained numerically using Eqs. 1 and 3. Point 3A in cross section A–A can be obtained by shifting point 3 along its helix line in the top view. The shift distance is

$$z_{33A}=z_3-z_{3A}=z_3-z_1, \tag{4}$$

Table 1 Calculation of the grinding data for the fluting operation

Location	First flute face grinding	Second flute face grinding
X	$-L_1 + Lw_2 \cos\phi - X_{f1}$	$-L_1 + Lw_2 \cos\phi - X_{f1}$
Y	$-Y_{f1} - y_d$	$-Y_{f2} - y_d$
Z_s	$-L_2 + L_t - Z_{f1} + Lw_2 \sin\phi + \delta Z$	$-L_2 + L_t - Z_{f2} + Lw_2 \sin\phi + \delta Z$
Z_e	$-L_2 + L_t - Z_{f1} + Lw_2 \sin\phi - l_c$	$-L_2 + L_t - Z_{f2} + Lw_2 \sin\phi - l_c$
B	ϕ	ϕ
C_s	0	$-\theta_s$
C_e	$180.\tan(h_e)(Z_e - Z_s)/D/2\pi$	$-\theta_s + 180.\tan(h_e)(Z_e - Z_s)/D/2\pi$

which can be obtained by using Eq. 2. The shift angle θ_{33A} in cross section A–A during shift (z_3–z_2) along the helix line with helix angle β is

$$\theta_{33A} = -\frac{(z_3 - z_1)\tan\beta}{R} \tag{5}$$

The polar coordinate of point 3A in the cross section can be determined using the following equation:

$$\begin{cases} r_{3A} = \sqrt{x_3^2 + y_3^2} \\ \theta_{3A} = \theta_3 + \theta_{33A} \end{cases} \tag{6}$$

Arbitrary point 2 along the wheel can be decided in the side view by increment Δz, using the following equation:

$$z_2 = z_1 + \Delta Z \tag{7}$$

When Δz is changed from 0 to (z_3–z_2), z_2 covers all the points between points 1 and 3. Point 2 can be determined by using Eqs. 1, 2, and 3. Point 2A must be shifted in the same way to find 2A in cross section A–A.

$$\begin{cases} r_{2A} = \sqrt{x_2^2 + y_2^2} \\ \theta_{2A} = \theta_2 + \theta_{22A} = \theta_2 + \dfrac{\Delta z \tan\beta}{R}. \end{cases} \tag{8}$$

Considering that a wheel with a finite thickness consists of thin wheels, as shown in Fig. 5, the groove configuration can be generated by accumulating the traces of each thin wheel. The center point of wheel O′ can be represented as follows:

$$\begin{cases} x_{o'} = x_o + t\ \cos\alpha \\ y_{o'} = y_o \qquad . \\ z_o' = -t\ \sin\alpha \end{cases} \tag{9}$$

The wheel can be expressed as

$$\frac{(x - x_{0'})^2}{(w'\sin\alpha)^2} + \frac{(y - y_{0'})^2}{w'^2} = 1 \tag{10}$$

and

$$\frac{(z - z_{o'})^2}{(w'\cos\alpha)^2} + \frac{(y - y_{0'})^2}{w'^2} = 1 \tag{11}$$

The configuration in cross section A′–A′ can be predicted through the same process as that used in the initial wheel. After predicting point 3A′ in cross section A′–A′, the polar coordinate of arbitrary point 2A′ is obtained using the following equations:

$$\begin{cases} r_{2A'} = \sqrt{x_{2'}^2 + y_{2'}^2} \\ \theta_{2A'} = \theta_{2'} + \theta_{22A'} = \theta_{2'} + \dfrac{\Delta z' \tan\beta}{R} \end{cases} \tag{12}$$

where $\Delta z'$ is the arbitrary increment from 0 to ($z_{3'}$–$z_{1'}$) in the side view. To see the groove in cross section A–A, all the points in cross section A′–A′ should be shifted to cross

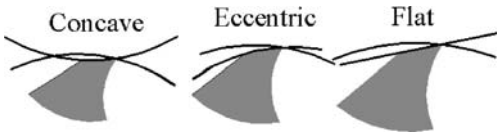

Fig. 10 Three cases of first clearance face grinding

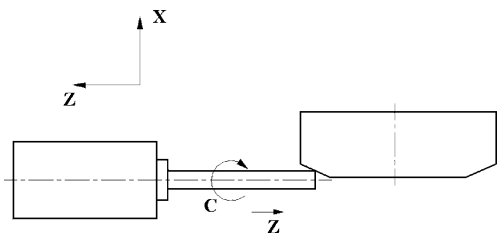

Fig. 11 Schematic diagram of the first clearance face grinding process

Table 2 Calculation of the data for clearance face grinding

Location	First clearance face grinding	Second clearance face grinding
X	$-L_1 + Lw_4 - \frac{T_4}{2} + \frac{D}{2}$	$-L_1 + \sqrt{\left(\frac{Dw_{1i}}{2}\right)^2 + Lw_1^2}\sin\gamma - \delta_2 + \frac{D}{2}$
Y	$-y_d$	$-y_d$
Z_s	$-L_2 + L_t + \frac{Dw_4 + Dw_{4i}}{4} + \delta Z$	$-L_2 + L_t + \sqrt{\left(\frac{Dw_{1i}}{2}\right)^2 + Lw_1^2}\cos\gamma + \delta Z$
Z_e	$-L_2 + L_t + \frac{Dw_4 + Dw_{4i}}{4} - l_c$	$-L_2 + L_t + \sqrt{\left(\frac{Dw_{1i}}{2}\right)^2 + Lw_1^2}\cos\gamma - l_c$
B	-180	ϕ
C_s	$180° - C_0 + \delta C$	$-(180 - \eta_2 - C_0) + \delta C$
C_e	$180 - C_0 + \frac{2.\tan(h_e)(Z_e - Z_s)180}{\pi D}$	$-(180 - \eta_2 - C_0) + \frac{2.\tan(h_e)(Z_e - Z_s)180}{\pi D}$

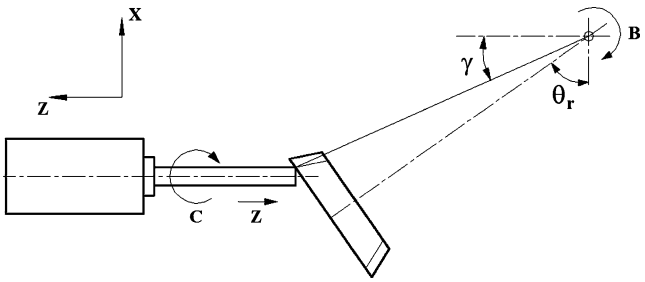

Fig. 12 Schematic diagram of the second clearance face grinding process

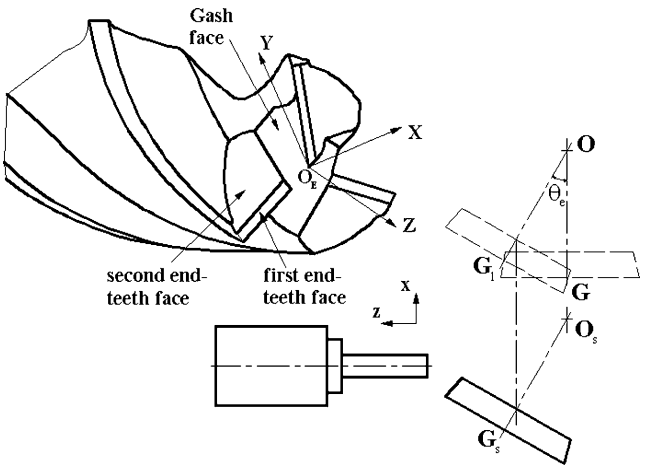

Fig. 13 Schematic diagram of the gash face grinding process

section A–A with the shift distance, calculated using the following equation:

$$\Delta z' = z_{1'} - z_1 \tag{13}$$

The cross section of the end mill is swept helically along the cylindrical shank. The equation of the helical-groove surface is

$$\begin{cases} x_f = x_c\cos\varphi + y_c\sin\varphi \\ y_f = y_c\cos\varphi - x_c\sin\varphi \\ z_f = z_c + \frac{P\varphi}{2\pi} \end{cases}, \tag{14}$$

where (x_c, y_c, z_c) and (x_f, y_f, z_f) are the positions of the points on the cross section and on the helical-groove surface of the end mill, and P is the pitch of the helix.

The relationship between the grinding wheel profile and the cross-sectional configuration of the end mill was discussed in [10]. Based on the relationship between Fig. 6a, b, rake face A′A″ in Fig. 6b was generated by wheel element A in Fig. 6a. Thus, the size of inclination angle θ_1 and thickness t_1 determined the cross-sectional configuration of the end mill in section A″B in Fig. 6b. Flute part BC1 was machined by wheel element BC in Fig. 6a. BC is the recess of the end mill. When the end mill does not contain a recess, such as the end mill for high-speed machining, the wheel without part BC is sometimes

Table 3 Calculation of the data for gash face grinding

Location	Gash face grinding
X_s	$-\left(L_1 - Lw_3\cos\theta_e + \left(\frac{Dw_{3i}}{2} + \delta G\right)\tan\theta_e\right)$
X_e	$-\left(L_1 - Lw_3\cos\theta_e + dX_1\tan\theta_e\right)$
Y_s	$-\left(\frac{Dw_{3i}}{2}\sin\theta_g - \frac{Dw_{3i}\left(1-\cos\theta_g\right)+2\delta G}{2\tan\theta_g}\right)$
Y_e	$-\left(\frac{Dw_{3i}}{2} + \delta G\right)$
Z_s	$-\left(\frac{Dw_{3i}}{2} + \delta G - \left(L_2 - L_t - Lw_3\sin\theta_g\right)\right)$
Z_e	$-\left(dX_1 - \left(L_2 - L_t - Lw_3\sin\theta_g\right)\right)$
B	$-180 - \theta_e$
C	$90 - C_0$

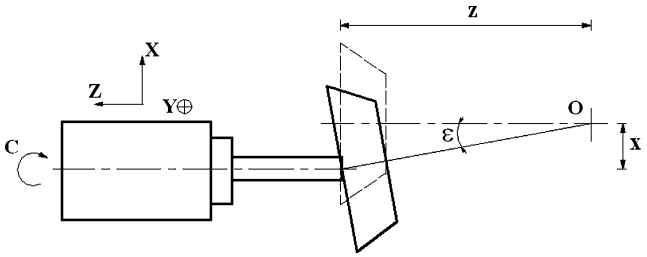

Fig. 14 Schematic diagram of the end teeth face grinding process

used. Figure 7 shows the cross-sectional plane of the flute and the rake as well as the clearance angle in the normal cross section of the end mill.

2.3 Grinding process for the flute surface

In the flute grinding operation, the program will determine the location of the wheel setting point for the first flute operation (x_0, y_0), contact point (x_{0f}, y_{0f}) between the wheel and the end mill, cross-point (x_1, y_1) between the grinding wheel and the outer diameter of the end mill, and the points on rake face (x_2, y_2), those on flute face (x_3, y_3), and the end points of flute (x_4, y_4).

The first step is to determine the wheel setting (x_0, y_0) to obtain predetermined rake angle γ. The starting point of the wheel in *Y*-axis y_0 must be given as the radius of the grinding wheel. The second step is to determine x_0 to satisfy the inscribed-circle diameter D_i. In this step, rake angle γ_t is calculated and compared with design value γ. The scanning location is changed by increasing the value $y_0 = y_0 + \Delta y_0$ until the calculated rake angle satisfies the design value within the desired margin of error. The second step is to determine the grinding wheel location (x_{02}, y_{02}) for the second flute operation to satisfy the maximum recess size in Fig. 8. If the wheel geometry does not allow the recess, this process of finding the proper value y_{0d} is unnecessary. In this case, the previous value of y_0 for the first flute operation will be used. In the second flute operation, the shift angle of the end mill rotation about the *Z*-axis is determined to configure the points on flute face (x_3, y_3). Figure 8 shows the configuration of the cross-sectional flute, which can be generated from the above processes by accumulating the grinding points in the fluting operation.

Figure 9 shows the relative movement between the grinding wheel and the workpiece in the grinding processes based on the coordinates of the machine and the workpiece. In each process, the initial and final positions are calculated. Considering the flute grinding process, the position in each axis can be calculated based on the schematic diagram for the helical-flute grinding process in Fig. 9a, b.

In the flute grinding process, the grinding wheel moves to the initial position (X_s, Y_s, Z_s) from its original position in Fig. 1. X, Y, and B can be calculated as in Table 1. The flute is ground when the workpiece moves along the *Z*-axis from Z_s to Z_e and rotates along the *C*-axis from C_s to C_e. During the helical-flute grinding process, the *B*-axis rotates by ϕ. Each position is calculated as in Table 1. In the second flute grinding process, the *B*-axis rotates by ϕ; from the starting point, the grinding wheel moves down in the Y

Table 5 Design parameters for the manufacturing performance of an end mill

Diameter	12mm
Number of teeth	4
Helix angle	30°
Rake angle	11°
D_i/D ratio	0.6
First clearance angle	3°
Second clearance angle	20°
Gash angle	40°
First end teeth angle	6°
Second end teeth angle	20°
Overall length	60 mm
Cutting length	20 mm

Table 4 Calculation of the data for end teeth face grinding

Location	First end teeth face grinding	Second end teeth face grinding
X_s	$-L_1 - Lw_1 \cos\phi - \left(\frac{Dw_1}{2}\right)\sin\phi\cos\varepsilon_{11} - -\frac{D}{2} - \delta E$	$-L_1 + Lw_1 + \frac{D}{2} + \delta X$
X_e	$-L_1 - Lw_1 \cos\phi - \left(\frac{Dw_1}{2}\right)\sin\phi\cos\varepsilon_{11}$	$-L_1 + Lw_1 - (D/16)$
Y	$-\left(\frac{Dw_1}{2}\right)\sin\varepsilon_{11} - y_d$	$-\left(\frac{Dw_1}{2}\right)\sin\varepsilon_2 + W_L - y_d$
Z_s	$-L_2 + L_t + Lw_1 \sin\phi + +\left(\frac{Dw_1}{2}\right)\cos\phi\cos\varepsilon_{11} + \delta E_t \tan\theta_b$	$-L_2 + L_t + \left(\frac{Dw_1}{2}\right)\cos\varepsilon_2$
Z_e	$-L_2 + L_t + Lw_1 \sin\phi + +\left(\frac{Dw_1}{2}\right)\cos\phi\cos\varepsilon - \left(\frac{D}{12}\right)\tan\theta_b$	$-L_2 + L_t + \frac{Dw_1}{2}\cos\varepsilon_2$
B	ϕ	0
C	$-C_0 - \delta C$	$180 - C_0 - \delta C$

Table 6 Calculation result of flute grinding

Wheel rotation angle (deg)	31.5
Rake angle (deg)	11.5
First clearance angle (deg)	3.00
Maximum ratio of recess (%)	99.75

direction to find the proper location y_d. After finding the proper position in the Y direction, the grinding wheel is fixed in the X and Y directions, and the workpiece rotates in the C direction from C_s to C_e and moves along the Z-axis from Z_s to Z_e. All the positions are calculated as in Table 1, where θ_s is the shift angle for the second flute operation.

2.4 Grinding process for the clearance faces

In general, end mills have three kinds of primary clearance angles, those with concave, eccentric, and flat shapes, as shown in Fig. 10. The shape of the primary clearance angle is based on the machining method and the grinding wheel geometry. In this study, the clearance face was machined as shown in Fig. 11 by using grinding wheels with an inclination angle; Eq. 15 shows the relationship among clearance angle (η), wheel inclination angle (θ_4), and helix angle (h_e).

$$\eta = \tan^{-1}\left(\frac{\tan\theta_4}{\tan h_e}\right). \tag{15}$$

For the first clearance face grinding, from its original position, the B-axis rotates by −180°, and the grinding wheel moves in the X and Z directions and then moves down in the Y direction to find the proper location y_d.

The starting point (X, Y_d, Z_s, B, C_s) can be calculated as in Table 2. Then the first clearance face is machined when the grinding wheel moves along the Z-axis from Z_s to Z_e and when the end mill rotates along the C-axis from C_s to C_e. The second clearance face is machined as shown in Fig. 12, using wheel number 1. From its original position,

Table 7 Calculation result of flute grinding (starting and ending positions)

Location	First fluting	Second fluting
X (mm)	−213.23	−208.27
Y (mm)	−156.68	−160.43
Z_s (mm)	−313.46	−322.18
Z_e (mm)	−372.18	−372.18
B (deg)	31.5	31.5
C_s (deg)	0	−16.93
C_e (deg)	−314.26	−331.19

Table 8 Influence of the rake angle on the helix angle

Helix angle (deg)	30	31	32	33	34
Rake angle (deg)	11.5	11.49	11.31	11.35	11.34

the B-axis rotates by ϕ; the workpiece rotates to C_s, and the grinding wheel moves in the X and Y directions to find the proper location y_d of the starting point (X, Y_d, Z_s, B, C_s). The grinding wheel is then fixed in the X and Y directions, and the workpiece rotates in the C direction from C_s to C_e and then moves along the Z-axis from Z_s to Z_e. All the positions were calculated as shown in Table 2.
where:

$$\gamma = 90^\circ - \left(\tan^{-1}\left(\frac{Dw_{1i}}{Lw_1}\right)\right) - \theta_r, \tag{16}$$

$$\delta_1 = \frac{D}{2}(1-\cos\eta_1) - \frac{Dw}{2}\sin\theta_r(1-\cos\psi_1), \tag{17}$$

$$\psi_1 = \sin^{-1}\left(\left(\frac{D}{Dw_{1i}\sin\theta_r}\right)\sin\theta_{c1}\right), \tag{18}$$

$$\psi_2 = \sin^{-1}\left(\frac{D-2\delta_1}{Dw_{1i}.\sin\theta_r}\right)\sin(\eta_2-\theta_m), \tag{19}$$

$$\delta_2 = \left(\frac{D}{2}-\delta_1\right)(1-\cos(\eta_2-\theta_m)) - \frac{Dw_m}{2} \times (1-\cos\psi_2), \tag{20}$$

$$Dw_m = Dw_{1i}.\sin\theta_r. \tag{21}$$

2.5 The grinding process for the gash face

Figure 13 shows the schematic diagram for the gash face grinding process. In the gash face grinding process, from its original position, wheel 3 rotates along the B-axis by $-180-\theta_e$ and moves in the X, Y, and Z directions to find the starting point of the gash face grinding process (point G_s) and then moves to the end point. Table 3 shows the calculation of the grinding data for gash face grinding.where:

$$dX_1 = \left(\frac{Dw_{i3}\cos\theta_g}{2} - \tan\theta_g\left(\frac{Dw_{i3}}{2}(1-\sin\theta_g)\right)\right) + \delta G. \tag{22}$$

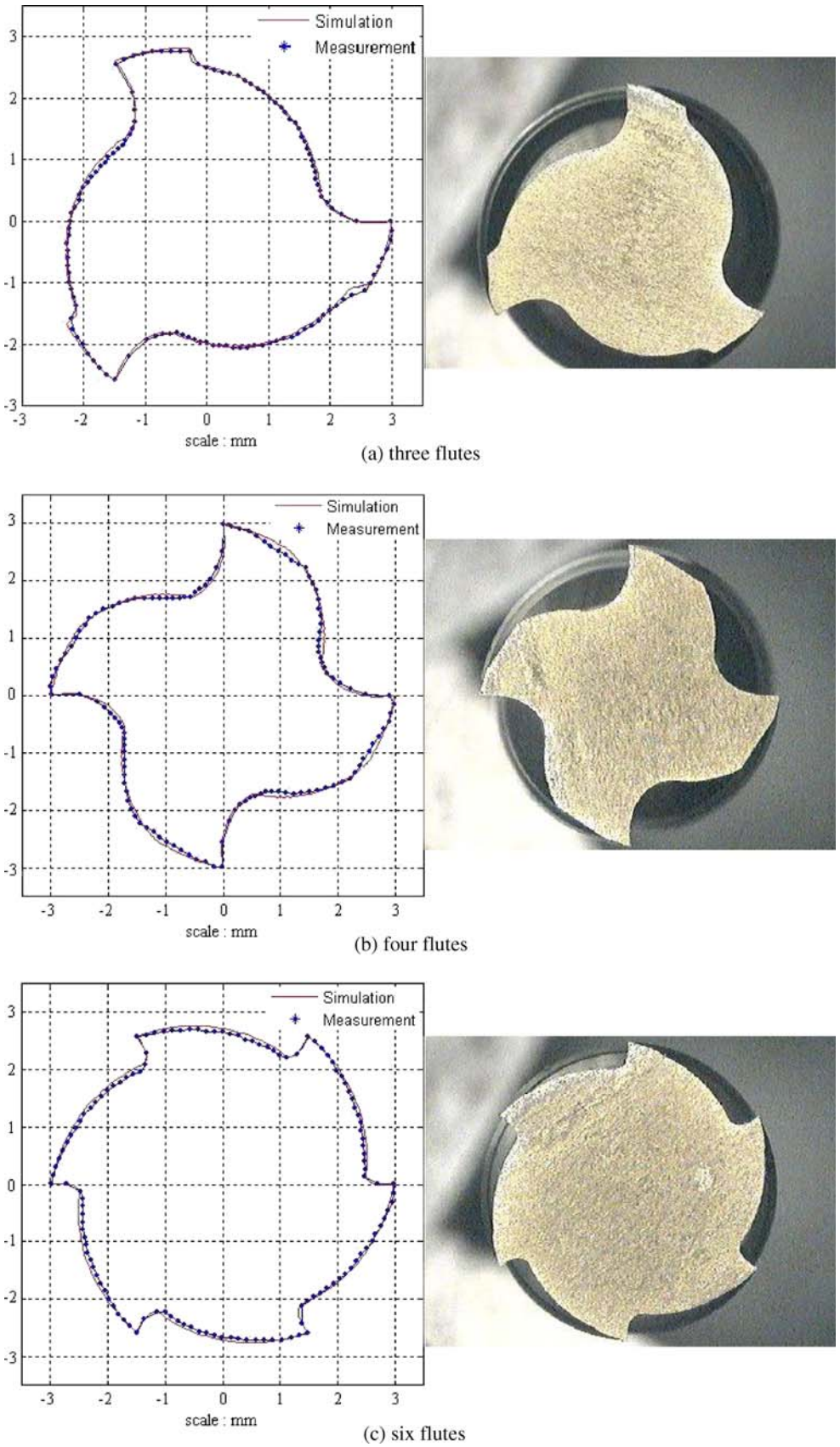

Fig. 15 Comparison of the simulation, measurement results, and machined cross-sectional profiles of the helical groove: **a** three flutes, **b** four flutes, **c** six flutes

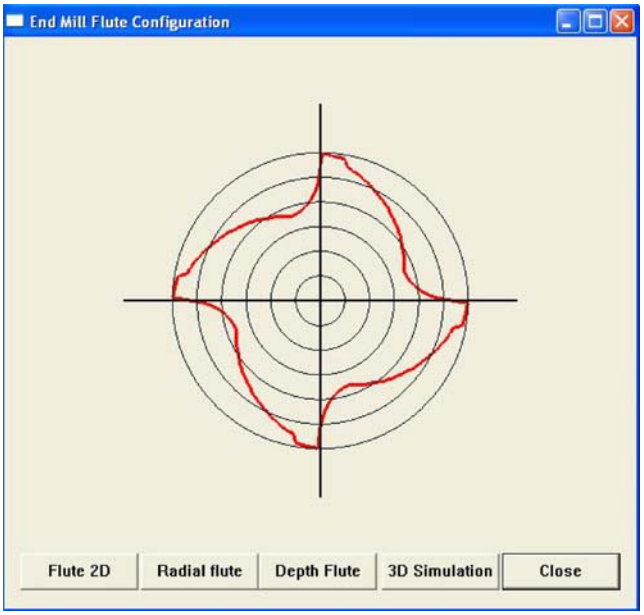

Fig. 16 Simulation result of the cross-sectional profile of the helical groove

2.6 Grinding process for the end teeth faces

The first end teeth face is machined using wheel number 1, as shown in Fig. 14. From its original position, the *B*-axis rotates by ϕ, and the grinding wheel moves to the starting point (X_s, Y, Z_s, B, C) and then moves along the *X*-axis from X_s to X_e and along the Z-axis from Z_s to Z_e.

Where

$$\varepsilon_{11} = \sin^{-1}\left(\frac{\sin\varepsilon_1}{\cos\phi}\right), \tag{23}$$

and θ_b is the back taper angle, a slight taper that makes the shank end of the cutting diameter smaller than the cutting end.

In the second end teeth face grinding process, from its original position, the grinding wheel moves in the X, Y, and Z directions to find the starting point (X_s, Y, Z_s, B, C) and then moves along the *X*- and *Z*-axes to the end point (X_e, Y, Z_e, B, C). Table 4 shows the calculation of the end teeth face grinding.

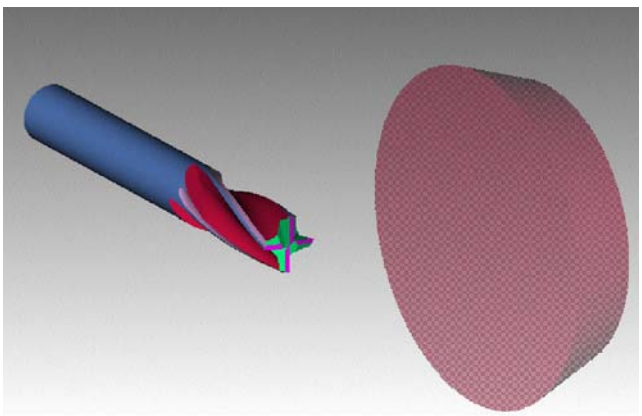

Fig. 17 3D simulation of the grinding processes

Fig. 18 Sample of an end mill machined using the developed software

3 Grinding performance and simulation results

3.1 Grinding performance and generation NC codes for end mill machining

In this section, the use of the suggested model for the performance of a grinding simulation for the end mill with the design parameters and cutting conditions in Table 5 is described. Moreover, the wheel geometry and machine setting parameters must be provided as input data. Using the input data for the end mill and grinding wheel geometries, the computer program will calculate and generate an NC code for all the grinding processes.

Tables 6 and 7 show the calculation results for the flute grinding process, including the starting and ending positions of the grinding wheel and the workpiece. The rake angle in Table 6 is different from that in Table 5 because it was obtained with some error due to the use of the trial and error method. Table 8 shows the influence of the helix angle on the rake angle.

Figure 15 shows the results of the comparison of the simulation (red line) and measurement (blue dotted line) results of the machined cross-sectional profiles in the following three cases, using the developed software: three flutes (Fig. 15a), four flutes (Fig. 15b), and six flutes (Fig. 15c). The simulation results coincide with the measurement results.

3.2 Simulation results

Using the data input, the computer program will calculate and generate the NC code for all the grinding processes,

which include the initial and final positions of each axis for all the processes. The NC code will be used to simulate all the machining processes in the three aforementioned dimensions.

Figure 16 shows the result of the simulation of the cross-sectional profile of the helical groove using the developed software, and Fig. 17 shows the result of the simulation of all the end mill grinding processes using Vericut. The simulation results ask for the users' views and measure all the geometry parameters of the end mill in any cross section to check and inspect whether they can achieve the designed end mill. Figure 18 shows the end mill sample, which was machined using the developed software.

4 Conclusions

The calculation, simulation, and experiment results indicate that the manufacturing model presented in this paper provides a simple and efficient method for technical programming to develop the computer software for the manufacture of a grinding end mill. The developed software based on the suggested manufacturing model is applied to design and manufacture end mills using five-axis CNC grinding machine. The prediction of the end mill geometry for the designing of the proper configuration of the end mill before manufacturing and generating the NC code for machining in a CNC machine is necessary to save time and to reduce the manufacturing cost.

Nomenclature

L_1, L_2	Machine setting parameters (L_1 is the distance between the face setup mandrel and the wheel, and L_2 is the distance between the circumference setup mandrel and the wheel)
Lw_1, Lw_2, Lw_3, Lw_4	Wheel locations from the center of the B-axis
Dw_1, Dw_2, Dw_3, Dw_4	Wheel diameters
L_T	Overall length of the end mill
l_c	Cutting-edge length
D	Diameter of the end mill
h_e	Helix angle
γ	Rake angle of the end mill
D_i	Inscribed-circle diameter of the end mill
D_r	Recess diameter of the end mill
η_1, η_2	First- and second-clearance angles
ϕ	Rotation of the wheel spindle (B-axis)
θ_m	Margin angle of the end mill
θ_r	Rotation of the wheel spindle in the second-clearance face operation
θ_e	Rotation of the wheel spindle in the gashing operation
ε_1, ε_2	First and second end teeth angles
θ_b	Back taper angle
θ_g	Gash angle
W_L	Land width
θ_s	Shift angle for the second flute operation
C_0	Initial angle of the C-axis
y_d	Destination location of the grinding wheel in the Y direction in the flute grinding process
X_{f1}, X_{f2}, Y_{f1}, Y_{f2}, Z_{f1}, Z_{f2}	The proper values of the grinding wheel in the fluting process in the X, Y, Z direction
X, Y, Z	Translation positions of the wheel and workpiece in the X-, Y-, and Z-axes
B	Rotation in the B-axis
Z_s, C_s	Initial translation and rotation in the Z- and C-axes
Z_e, C_e	Final translation and rotation in the Z- and C-axes
δX, δY, δZ, δC	Increment of the relative movements between the wheel and the workpiece in the X-, Y-, Z-, and C-axes
δG, δE_t	Increment of the relative movements between the wheel and the workpiece during the gash face and end teeth face grinding processes

Acknowledgement This work was accomplished with support from the Seoul R&BD program (10848) and the Korean Foundation for International Cooperation of Science & Technology (KICOS), through grant no. K20701040597-07A0404-05110 from the Korean Ministry of Education, Science, and Technology (MEST).

References

1. Kang SK, Ehmann KF, Lin C (1996) A CAD approach to helical groove machining, part 1: mathematical model and model solution. Int J Mach Tools Manuf 36:141–153
2. Chen CK, Lin RY (2001) A study of manufacturing models for ball-end type rotating cutters with constant pitch helical grooves. Int J Adv Manuf Technol 18:567–578
3. Wu CT, Chen CK (2001) Study on rotating cutters with different definitions of helical angle. Int J Adv Manuf Technol 17:627–638
4. Chen WF, Lai HY, Chen CK (2001) A precision tool model for concave cone end milling cutters. Int J Adv Manuf Technol 18:567–578
5. Kang D, Armarego EJA (2003) Computer aided geometric analysis of the fluting operation for twist drill design and production, part I: Forward analysis and generated flute profile. Mach Sci Technol 7(2):221–248
6. Zhang W, Wang X, He F, Xiong D (2006) A practical method of modelling and simulation for drill fluting. Int J Mach Tools Manuf 46:667–672

7. Hsieh JF (2006) Mathematical model and sensitivity analysis for helical groove machining. Int J Mach Tools Manuf 46:1087–1096
8. Lu Y, Takeuchi Y, Takahashi I, Anzai M (2005) An integrated system development for ball end mill design, creation, and evaluation. Int J Adv Manuf Technol 25:628–646
9. Xu ZG, Zhao B (2006) A research on the design and management of the carbide end mill. Proceedings of the SICE-ICASE International Joint Conference, IEEE Xplore, http://ieeexplore.ieee.org/xpls/abs_all.jsp?arnumber=4108134
10. Ko S. L. (1994) Geometric analysis of helical flute grinding and application to end mills. Trans. NAMRI/SME, XXII
11. Kim YH, Ko SL (2002) Development of a design and manufacturing technology for the end mill in machining-hardened steel. J Mater Process Technol 130–131:653–661